Fuel 313 (2022) 122674

Contents lists available at ScienceDirect

Fuel

journal homepage: www.elsevier.com/locate/fuel

Full Length Article

Flammability enhancement of swirling ammonia/air combustion using AC powered gliding arc discharges

Yong Tang [a], Dingjiang Xie [a], Baolu Shi [a,*], Ningfei Wang [a], Shuiqing Li [b]

[a] School of Aerospace Engineering, Beijing Institute of Technology, Beijing 100081, China
[b] Key Laboratory for Thermal Science and Power Engineering of Ministry of Education, Department of Thermal Engineering, Tsinghua University, Beijing 100084, China

ARTICLE INFO

Keywords:
Plasma-assisted combustion
Ammonia combustion
Swirling flame
Lean blow-off limit
NO_x emission

ABSTRACT

Aiming at the potential development of ammonia as a carbon-free renewable fuel, this work investigates the flammability and NO_x emission of swirling ammonia/air flames and utilizes plasma to enhance ammonia combustion. First, the well-designed rapidly-mixed swirl burner can anchor compact ammonia/air flames under a wide range of flow conditions, with the current maximum heat release of approximately 4.7 kW. The flame is progressively detached from the quartz confinement tube and goes blow-off when the equivalence ratio drops below approximately 0.7–0.8. Then, to alleviate the problem of low flammability, gliding arc discharges driven by a 12.5 kHz alternating current (AC) power supply are facilitated to extend the lean blow-off margin to approximately 0.3–0.4. The localized flame kernels surrounding the discharge column are detected by high-speed photography. The planar laser-induced fluorescence (PLIF) imaging of OH radicals, optical emission spectroscopy, and NH_2* chemiluminescence measurement are performed to interpret the intermediate chemistry. Finally, the NO_x emission of the swirling ammonia/air flame is measured by a flue gas analyzer. Results show that although the AC-powered gliding arc exhibits weak global effects on the NO_x reduction of burner-stabilized ammonia/air flames prevailing at higher equivalence ratios (*e.g.*, $\varphi > 0.75$), leaner flames stabilized by discharges can achieve NO_x emissions below 100 ppm due to the thermal DeNO_x mechanism.

1. Introduction

As a carbon-free hydrogen carrier, ammonia (NH_3) is a promising candidate for sustainable and renewable fuel to address some global challenges such as energy shortage and climate change [1–2]. Ammonia can be synthesized by harvesting renewable power sources through a carbon-free process. Comparing to hydrogen, ammonia takes advantage of easier production, distribution, and utilization capacity, as well as more reliable infrastructure to support the future energy mix [3]. The use of ammonia as a fuel can be traced back to the last century, such as the Belgian buses that used ammonia instead of diesel [4] and NASA's X-15 airplane that burned ammonia and liquid oxygen [5]. Kobayashi *et al.* [6] and Li *et al.* [7] reviewed the investigation and development of ammonia combustion technologies in recent years. Japan has realized industrial power generation from ammonia combustion in a 155 MW coal-fired power plant and a 50-kW class micro gas turbine [8], respectively. A great number of fundamental studies on ammonia combustion have been devoted to interpreting the oxidation mechanisms [9], flame structures [10–11], ignition characteristics [12], NO_x emissions and associated kinetics [13].

However, issues associated with combustion efficiency and flammability range are currently a barrier to the implementation of ammonia as a primary fuel. Basically, comparing to common hydrocarbon fuels, ammonia combustion shows longer ignition delay, higher ignition temperature, lower flame temperature, and narrower flammability [6]. The heat release and maximum laminar flame velocity of ammonia/air combustion are approximately 40% and 20% of a conventional hydrocarbon flame, respectively. In addition, ammonia combustion also faces the challenge of high fuel NO_x emissions. To circumvent these difficulties, swirling flows were introduced downstream of ammonia/air combustors to generate recirculation zones stabilizing turbulent ammonia/air flames at various pressures [14–15], while the range of flame operating conditions was still limited [16].

Blending common fuels such as CH_4 or H_2 can further improve the burning velocity and flammability of ammonia/air combustion [17–19]. For example, Han *et al.* and Tang *et al.* experimentally proved that blending NH_3 with H_2 could improve the laminar burning velocity and blow-out limits of NH_3 flame [20–21]. Li *et al.* reported that adding H_2

* Corresponding author.
E-mail address: shibaolu@bit.edu.cn (B. Shi).

https://doi.org/10.1016/j.fuel.2021.122674
Received 7 October 2021; Received in revised form 17 November 2021; Accepted 19 November 2021
Available online 1 December 2021
0016-2361/

could increase the heat release rate of NH_3 flames through transport and chemical effects [22]. Zhang *et al.* and An *et al.* investigated the regulation effect of hydrogen and methane on NO emissions of ammonia/air swirling flames [23–24]. Kurata *et al.* tested NH_3/CH_4/air combustion in a 50-kW class gas-turbine, in which NO emissions first increased and then decreased as the NH_3 fuel ratio increased [8]. These works demonstrated that blending NH_3 with CH_4 and H_2 could increase the feasibility of NH_3 in industrial combustion. However, blending fuel may introduce more carbon emissions or increase the cost of fuel transportation and storage [25].

Another promising strategy to enhance fuel flammability is plasma-assisted combustion (PAC) [26–28]. Prior studies on common hydrocarbon fuels have proven that PAC can enhance the ignition and burning process [29–30], extend extinction limits [31–32], suppress combustion instabilities [33], and reduce pollutant emissions [34]. For turbulent swirling flames under high-speed, ultra-lean, or pulsating conditions, the repetitively pulsed discharges and AC-powered gliding arc discharges show good performance in flame stabilization and flammability extension [35–39]. Regarding plasma-assisted ammonia combustion, Shioyoke *et al.* found that plasma could increase the ammonia decomposition rate and laminar burning velocity [40]. Faingold and Lefkowitz reported that plasma could reduce the ignition delay time by 40–60% [41]. Recently, Choe *et al.* experimentally demonstrated that nanosecond pulsed discharges (NPD) could extend the lean blow-off limits and reduce NO_x emissions of swirling premixed ammonia/air flames [42]. However, they suggested that the coupling effect of plasma and ammonia combustion was new and largely unknown, and further studies were required.

Therefore, this work seeks to implement plasma in a laboratory-scale swirling burner to alter ammonia combustion. Instead of NPD that may cause severe electromagnetic interference, this work utilizes AC-powered gliding arcs (GA) to allow thermal and non-thermal enhancement. Due to the complexity of flame and discharges, in-situ optical diagnostics are performed to investigate the intermediate chemistry of plasma and combustion, including planar laser-induced fluorescence (PLIF) imaging of OH radicals, high-speed photography, spectrometer inspection, and NH_2* chemiluminescence measurements. Finally, a flue gas analyzer is employed to measure NO_x emissions of ammonia flames with and without gliding arc discharges.

2. Experimental methodologies

2.1. Burner and electrodes

Fig. 1 shows the schematic and images of the swirling flame burner integrated with electrodes. As illustrated in Fig. 1(b), the swirler consists of four tangential slits with an inner diameter of 16 mm and a slit width (W) of 2 mm, giving a swirl number of about 0.7 [43]. A cylindrical quartz tube, with an inner diameter of 48 mm and a height of 100 mm, was installed to create a confined space. Schematics of the inner recirculation zone (IRZ), the outer recirculation zone (ORZ), and the shear layer region are indicated in Fig. 1(a). Fig. 1(b) shows that gaseous NH_3 and air are individually injected from two parallel slits and rapidly mixed before entering the combustion chamber. The ammonia flow rate controlled by a mass flow controller varies between 0 and 20 L/min. Assuming complete combustion of ammonia, the peak energy power reaches approximately 4.7 kW.

The copper electrodes, including the central high-voltage rode and outer grounded nozzle, generate gliding arcs that move with the swirling flow. The central rod with a maximum diameter of 12 mm also acts as a flame stabilizer. Two ceramic dielectric plates were installed to fix the swirler and electrodes. The gliding arc discharge was facilitated by an AC power supply with an operating frequency of approximately 12.5 kHz. The voltage and current waveforms were measured by a Tektronix P6015 probe and a Pearson 2877 probe placed midway on the cable, respectively, and recorded by a Pintech oscilloscope. Fig. 1(c) and Fig. 1

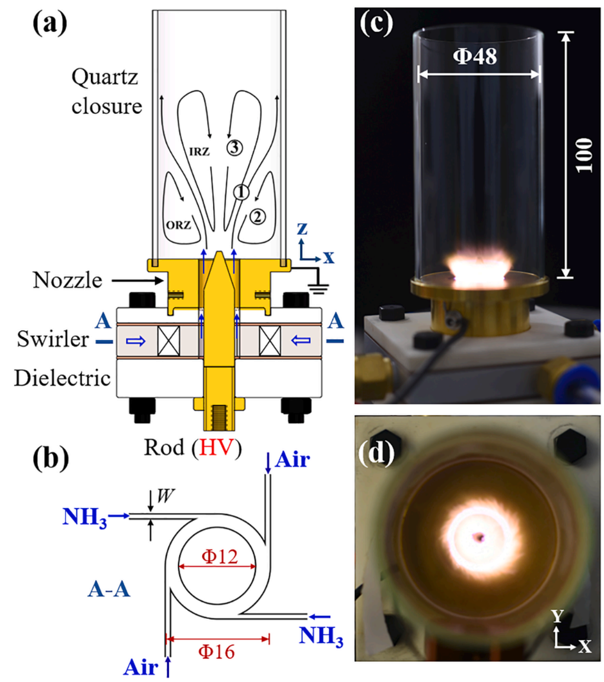

Fig. 1. Schematics of (a) the swirling burner integrated with electrodes and (b) flow injections; images of the burner and gliding arc discharges in air (Q_{air} = 50 slm) from (c) the side view and (d) the top view.

(d) show images of the gliding arc plasma sustained in air (Q_{air} = 50 slm) from the side and top view, respectively.

Fig. 2 shows typical voltage and current waveforms of gliding arc discharges sustained in an air flow of 50 slm. The breakdown that occurs at each half alternating cycle is indicated by the voltage kink [44]. The breakdown voltage changes from approximately 1 kV to 4 kV due to the variation of arc column length [45]. Unlike the voltage drop immediately after breakdown, the current wave presents a more continuous jagged shape. The peak current is approximately 0.25 A, except for a few random peaks>0.5 A. The energy deposition calculated by integrating the product of the voltage and current waveforms is approximately 200 W. The mixture composition will affect the discharge process. Generally, with the assistance of discharge, the mixture with a higher equivalence ratio can react to generate more heat and charged species, which can reduce the breakdown threshold. The plasma-combustion interaction is a closed-loop feedback process that can self-sustain high-temperature kernels [46]. The deposited energy drops to approximately 150 W once the flame is ignited, which is close to 3% of the maximum power released by the ammonia swirling flame at Q_{NH3} = 20 slm.

2.2. Diagnostics

Fig. 3 shows a schematic of the diagnostics, including the OH PLIF system, cameras, and a flue gas analyzer. The planar laser-induced fluorescence (PLIF) system was used to visualize OH distributions. The 10 Hz Nd: YAG nanosecond pulsed laser (Spectra-Physics LAB-190–10) produces 532 nm beams to pump the dye laser (Sirah CobraStretch) and double frequency crystal (BBO), generating 283 nm beams with an energy output of ~ 15 mJ/pulse. Passing through the optical lens, the beam expands to a planar sheet with a height of ~ 60 mm and a thickness of ~ 0.5 mm. The OH signal was recorded by an enhanced charge-coupled detector (ICCD, LaVision Imager SX 4 M) integrated with an OH filter. The PLIF image was background corrected and post-processed using the LaVision system, during which the energy non-uniformity of the laser sheet was also corrected.

In addition to PLIF, ICCD was integrated with a 632 ± 10 nm

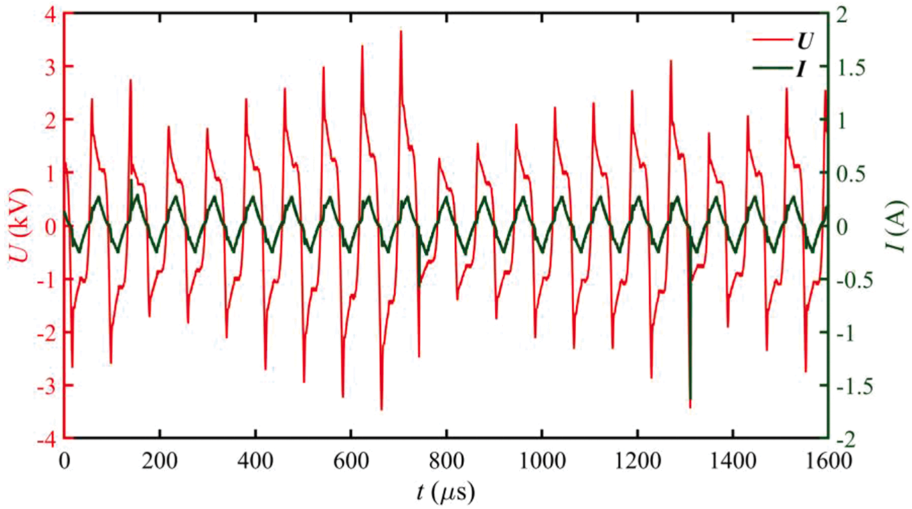

Fig. 2. Typical voltage and current waveforms of gliding arc discharges in air (Q_{air} = 50 slm).

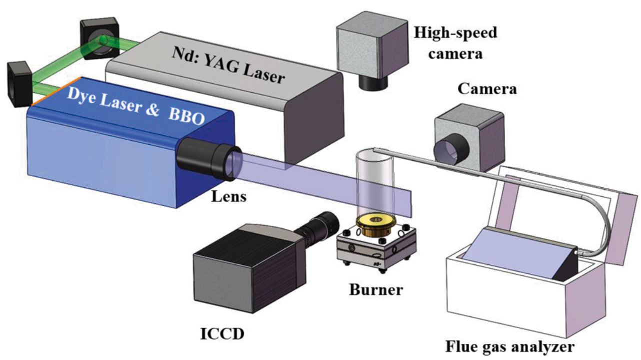

Fig. 3. Schematic of diagnostics including the OH PLIF system, cameras and a flue gas analyzer.

bandpass interference filter to capture NH_2* chemiluminescence signals near 630 nm. Besides, a fiber spectrometer (Ocean Optics), with an optical resolution of ~ 0.4 nm, was used to record the emission spectrum from gliding arcs and ammonia flames. The wavelength and relative intensity response of the spectrometer were pre-calibrated. Moreover, a Phantom high-speed camera and a Nikon digital camera were employed for visual inspections at different exposure times and frame rates. It is noted that the emission of ammonia flame in the visible range is strong enough that the high-speed camera can capture sufficient flame signals at a frame rate of 5 kHz.

Further, a flue gas analyzer (ECOM-EN3) feeding on gas exhaust at a flowrate of ~ 2 L/min (standard condition) was utilized to measure NO and NO_2 emission near the burner outlet. A 1.2-meter stainless tube was employed as a sampling gun to collect high-temperature exhaust and cool it before entering the analyzer. The head of the sampling gun was placed at the centerline and approximately 10 mm away from the outlet of the quartz tube (X = Y = 0, Z = 110 mm).

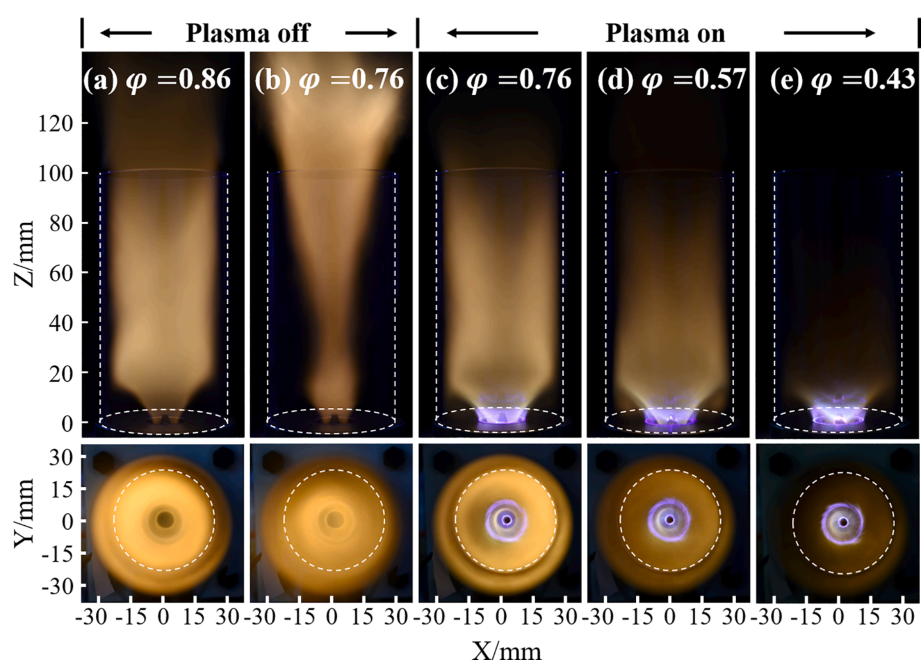

Fig. 4. Typical images of swirling ammonia flame at different equivalence ratios and Q_{air} = 50 L/min, in the absence and presence of plasma.

3. Results and discussion

3.1. Flammability limits of ammonia/air swirling flames

Fig. 4 shows typical images of swirling ammonia flames under different equivalence ratios and discharge conditions, taken by a Nikon digital camera at an exposure time of 1/5 s. The ammonia flame at different equivalence ratios shows orange/yellow hue typically due to the emission from NH_2*excited radical and the superheated water vapour spectrum [47]. The equivalence ratio is calculated based on the overall reaction of NH_3 with O_2:

$$4NH_3 + 3O_2 \rightarrow 2N_2 + 6H_2O \quad (1)$$

Fig. 4(a) shows that at $\varphi = 0.86$, the swirling flame attached to the central rod and quartz wall is stable. When the equivalence ratio decreases to 0.76, as illustrated by Fig. 4(b), the flame is still anchored at the central rod but detached from the wall. This cone-shaped flame is not stable and sometimes oscillates in the quartz closure. The flame will go blow-off as the equivalence ratio further decreases. Fig. 4(c) shows that the flame at $\varphi = 0.76$ is attached again when the plasma is turned on. Even the equivalence ratio drops to 0.57, as Fig. 4(d) shows, the flame is still stable. As the equivalence ratio drops to extremely low (*e.g.*, $\varphi =$ 0.43), the flame signal sustained by the gliding arc becomes very weak. Flame blow-off in the presence of plasma is defined as the moment when almost no flame signals can be detected above the arc column (Z > 10 mm).

Fig. 5 summarizes the detachment and flammability limits of swirling ammonia flames at air flow rates of 20–80 slm, corresponding to the Reynolds number of approximately 1500–6000. The uncertainty bar includes the uncertainty from the flowmeter (~1.5%) and the random error from at least three repeated measurements. As illustrated in Fig. 4, the ammonia swirling flame is detached from the wall before blow-off. The detachment limit increases from ~ 0.72 to ~ 0.85 as the air flow increases from 20 to 80 slm, while the blow-off limit increases from ~ 0.67 to ~ 0.82, indicating a narrow equivalence ratio range between flame detachment and blow-off. The relatively poor stabilization performance of NH_3/air results from the small laminar burning velocity and low heat release rate [6]. When the plasma is turned on, the flame will never appear as the cone-shaped flame shown in Fig. 4 (b). In the presence of plasma, Fig. 5 only plots the blow-off limits and demonstrates that the gliding arc discharge significantly extends the lean blow-off limit to approximately 0.32–0.4 within the air flow range of 20–80 slm. The extension of the lean blow-off limit by plasma is somewhat better than that achieved by blending methane or hydrogen [16,23].

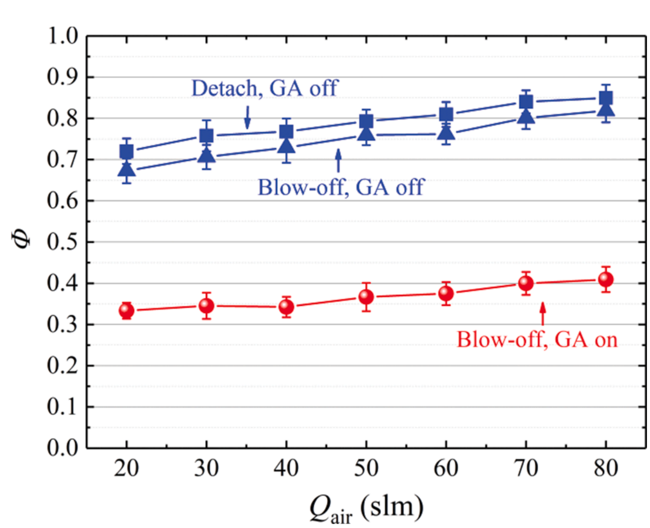

Fig. 5. Detach and flammability limits of swirling ammonia flame at air flow rates (Q_{air}) of 20–80 slm, corresponding to the Reynolds number of 1,500–6,000.

Further, a high-speed camera was used to visualize the repetitive local ignition process of gliding arcs from the top view. The frame rate of 5 kHz has the same magnitude as the operating frequency of the discharge (~12.5 kHz). Fig. 6 shows typical continuous images of swirling ammonia flames in the absence and presence of plasma. Without plasma, the annularly distributed flame signals show wrinkled structures due to the swirling and turbulent flow. As the equivalence ratio decreases to 0.76, the cone-shaped flame (see Fig. 4b) contracts and detaches from the wall. When the discharge is turned on, the flame is reattached. The arc column can be easily distinguished as bright emissions along the plasma column. The enhanced flame signal surrounding the plasma can last for a few milliseconds. Under extremely lean conditions ($\varphi = 0.43$), the local flame kernel induced by the arc column is difficult to propagate outward to form a larger flame area, confirming the flammability limit of ammonia flames in the presence of gliding arcs.

The NH_3/air flame behaviors and responses to gliding arc discharges are somewhat similar to those of CH_4/air swirling flames reported in previous work [39]. In particular, the plasma stabilizes swirling NH_3/air and CH_4/air flames by repetitive local ignition effects through heat deposition and active species pools. The body force and flow fluctuations induced by plasma are relatively small for high-speed flow with large inertial forces (*e.g.*, Re > 1500) [44]. The gas temperature surrounding the plasma column is generally>1000 K at atmospheric pressure [48]. Active species include high-energy electrons, radicals such as O/H/OH, and excited oxygen and nitrogen molecules [30]. In the positive feedback loop, the heat release and discharged species produced by fuel oxidation promote the discharge. As explored by Miller *et al.* [49] and reviewed by Kobayashi *et al.* [6], NH_3/air combustion is primarily initiated by the H abstraction effect where NH_3 reacts with OH radicals. In addition, the reactions with H and O produce NH_2, while the oxidation of NH_i ($i = 0,1,2$) results in NO production or reduction. Therefore, the key intermediates, including H, O, OH, and NH_2, are detected through optical diagnostics to better understand the ammonia flame dynamics, emissions, and responses to plasma in the following section.

3.2. Key intermediates

Fig. 7 shows the emission spectra of plasma and flame in the 500–930 nm wavelength range. The exposure time for the acquisition of each spectra curve is 1 s, covering approximately 12,500 discharge cycles. In air flow ($\varphi = 0$), the first line (L_1) shows characteristic peaks near 778 and 844 nm from the atomic emission of oxygen $O(^5P)$ and $O(^3P)$, respectively. At higher equivalence ratios, the second line (L_2) and the third line (L_3) add signals near 656 nm from the atomic emission of hydrogen H_α. These peaks indicate that the plasma promotes the dissociation of oxygen and ammonia molecules. On the other hand, for a stable flame without plasma (L_5), the signal from NH_2 (α band, $^2A_1$-$^2B_1$) contains multiple lines extending throughout the visible and near infrared, including peaks near 632 nm and a strong head near 734 nm [50]. In addition, the water vapour, as the product of NH_3 oxidation, also emits strong signals near 890 and 930 nm, while the peak near 930 nm is cut in Fig. 7. The fourth line (L_4) indicates that the presence of gliding arcs does not change the spectrum over 500–930 nm significantly, except for the addition of peaks from H/O atoms. The H/O radicals play a role in the dominant chain reaction of NH_3/air [19,51]:

$$NH_3 \rightarrow NH_2 \rightarrow NH \rightarrow N \rightarrow N_2 \quad (2)$$

where NH_3 is finally converted to N_2 and H_2O.

As an essential intermediate of NH_3 oxidation, the chemiluminescence from self-excited NH_2 was captured by an ICCD camera equipped with a 632 nm bandpass filter. After background correction, the line-of-sight integrated chemiluminescence intensity was processed using a modified Abel inversion algorithm assuming azimuthal

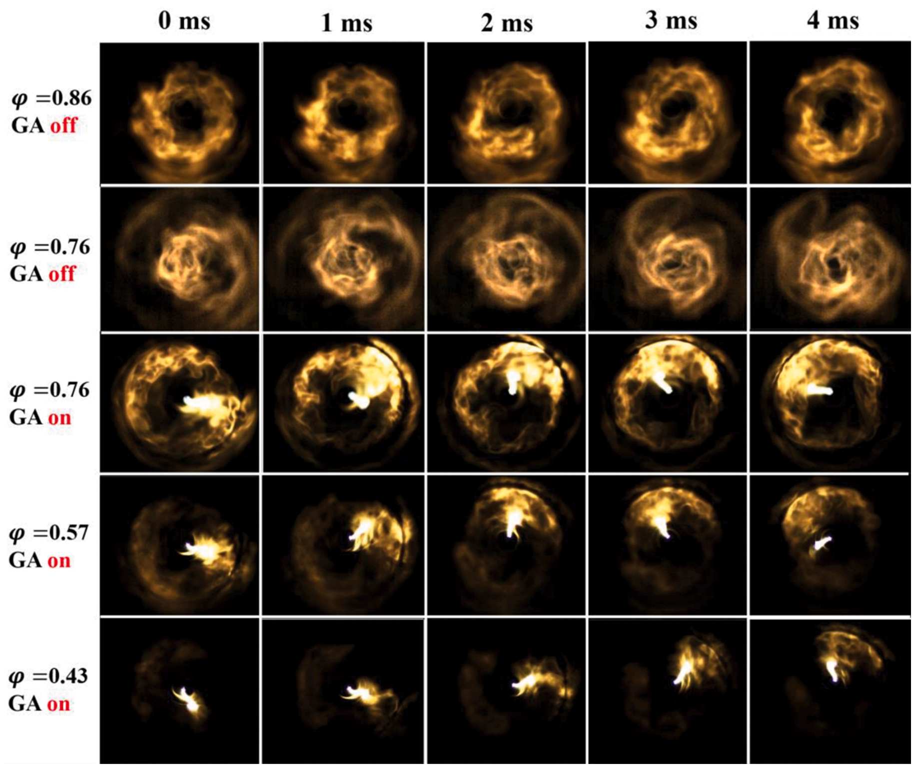

Fig. 6. High-speed photography of swirling ammonia/air flames in the absence and presence of gliding arcs (GA), at Q_{air} = 50 slm and different equivalence ratios, with a frame rate of 5 kHz and an exposure time of ~ 200 μs.

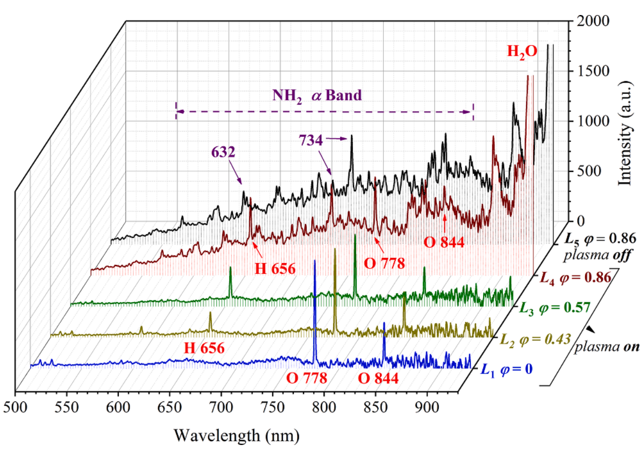

Fig. 7. Emission spectra of plasma and ammonia flames at Q_{air} = 50 slm and different equivalence ratios.

symmetry [10]. Fig. 8 shows the Abel-transformed and time-averaged images of NH_2* chemiluminescence from swirling ammonia/air flames. It should be noted that there are weak signals in an approximate triangular region (-25 < X < 0, 0 < Z < 20) in Fig. 8(e-g) due to the asymmetry caused by gliding arcs. At a higher equivalence ratio, the signal is mainly distributed at the shear layer and the area close to the wall. As the equivalence ratio decreases to 0.76 approaching the blow-off limit, the signal becomes weaker in the absence of plasma. The second row in Fig. 8 verifies that the plasma can reignite and hold flames at a smaller equivalence ratio. In the surrounding reactants, the plasma can directly trigger NH_3 dissociation that produces NH_2 and NH through electron impacts [41]:

$$e + NH_3 \rightarrow e + NH_2 + H \tag{3}$$

$$e + NH_3 \rightarrow e + NH + H + H \tag{4}$$

In particular, comparing Fig. 8(d) and Fig. 8(e) at the same equivalence ratio of 0.76 indicates that the arc increases local signals along the shear layer, making the flame reattach to the wall. As the equivalence ratio further drops, the residual NH_2* signal along the shear layer becomes shorter.

The OH PLIF imaging was performed to interpret the dynamics and kinetics of ammonia/air swirling flame approaching blow-off. Fig. 9 illustrates the OH PLIF signals of ammonia/air flames without discharges, including time-averaged images of 100 single-shots and typical single-shot images illustrating instantaneous structure. The OH signal is mainly distributed near the shear layer and in the inner recirculation zone. Different from methane/air flames, the OH signal of ammonia/air swirling flame peaks at the equivalence ratio of approximately 0.8–0.86 in this work. The signal obtained at the equivalence ratio of 0.92 becomes quite weak. When the flame is close to blow-off (φ = 0.76), the OH PLIF structure is completely detached and exhibits hollow structures downstream of the inner recirculation zone.

In comparison, Fig. 10 shows OH PLIF signals of ammonia flames enhanced by gliding arc discharges. The OH PLIF signal becomes stronger due to the plasma-induced O/H radical pools from the dissociation of fuel and oxygen [29]. Fig. 10 (a) shows that the OH structure is reattached to the wall with the assistance of plasma. At φ = 0.57, Fig. 10 (g) indicates that sufficient OH PLIF signals can still be detected, although the fragmented signal is detached from the wall. When the equivalence ratio decreases to 0.43, Fig. 10(d) and Fig. 10(h) show that few OH signals are observed in the recirculation zones. Some residual signals can be detected near the shear layer and along the arc column.

The OH radical plays an important role in the initiation of ammonia oxidation [51]:

$$NH_3 + OH \leftrightarrow NH_2 + H_2O \tag{5}$$

$$NH_2 + OH \leftrightarrow NH + H_2O \tag{6}$$

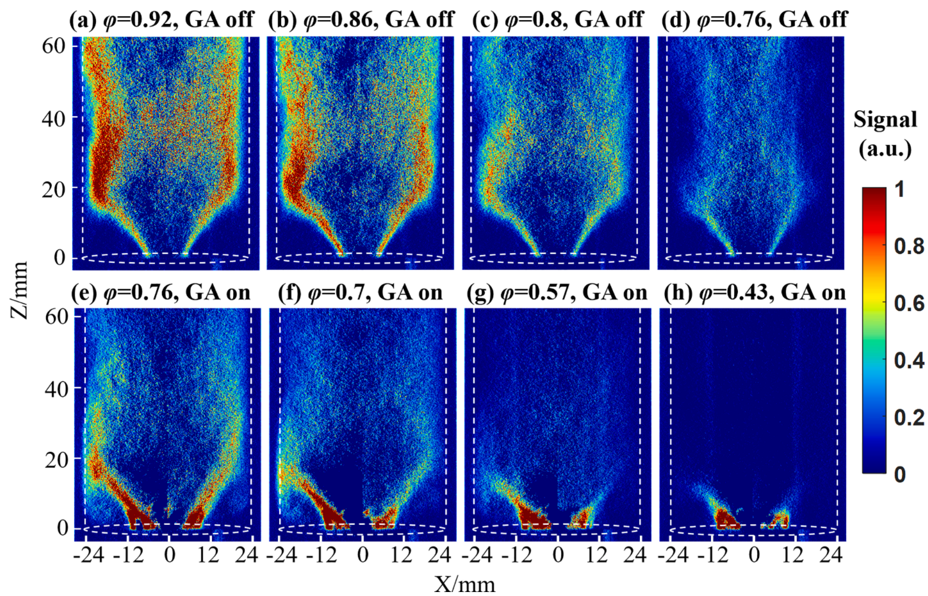

Fig. 8. Abel-transformed and time-averaged image of NH_2* chemiluminescence from swirling ammonia flames without plasma (a-d) and with plasma (e-h), at Q_{air} = 50 slm and different equivalence ratios. The outline of the quartz closure is indicated by dashed lines.

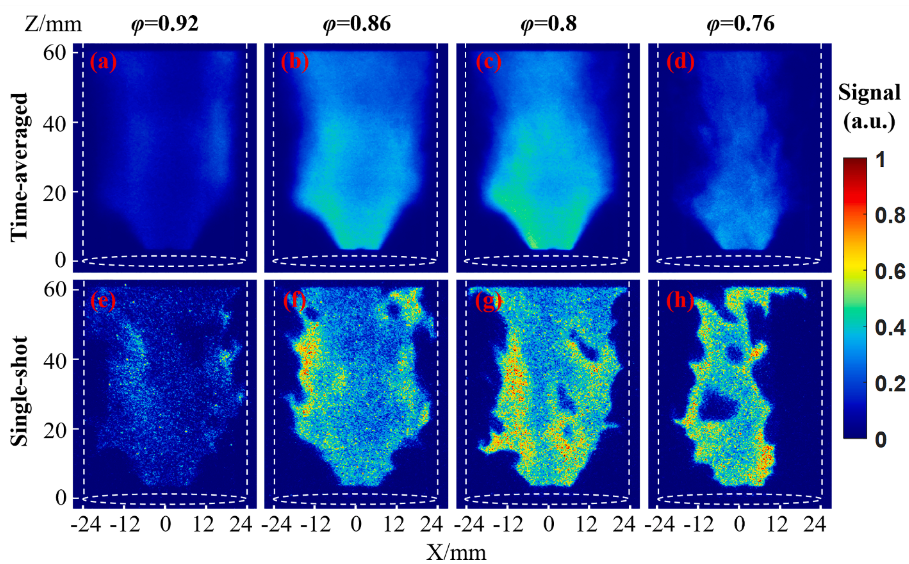

Fig. 9. Time-averaged (a-d) and typical single-shot (e-h) OH PLIF imaging of swirling ammonia/air flames without plasma, at Q_{air} = 50 slm and different equivalence ratios. The outline of the quartz closure is indicated by dashed lines.

These chain reactions with OH radicals are closely associated with the heat release of ammonia combustion. It is noted that the main chain reactions shown in Eqs. (2) act as chain termination reactions that consume O/H/OH radicals. Therefore, particularly at very lean conditions, the O/H/OH radical pools supplied and sustained by plasma will produce significant kinetic effects on NH_3 ignition by accelerating the chain reactions. Detailed kinetics governing plasma-assisted ignition and oxidation of NH_3 has been discussed in Ref. [41] through a zero-dimensional numerical model.

3.3. NO_x emission

Figs. 11 and 12 show NO and NO_2 emissions measured by the flue gas analyzer, which illustrate similar trends as the equivalence ratio increases from zero to one, since NO_2 formation mainly depends on the oxidation reaction of NO [51]. The concentration of NO_2 is smaller than that of NO by more than an order of magnitude. The emission of NO and NO_2 peaks near the equivalence ratio of approximately 0.8, where NO emission reaches approximately 1500 ppm. This differs from CH_4/air flames where the maximum NO emission of 100–200 ppm is generally obtained near the stoichiometric condition ($\varphi = 1$). For NH_3/air flames, N atoms come from the fuel, and NO emission is strongly associated with NH_2. The concentration of O/H/OH radicals affects the pathway of NH_2 oxidation, which can result in the production of NO through the HNO intermediate channel, or cause NO consumption through NO + NH_i (i = 0,1,2) reactions [6]. In particular, Somarathne *et al.* suggested a linear correlation between local NO emission and local OH concentration at various equivalence ratios [51]. Due to prevalent O/H/OH radicals that favor NO production in lean ammonia/air flames, the NO concentration peaks around the equivalence ratio of 0.8–0.85, which is consistent with the OH intensity at different equivalence ratios in Fig. 9.

Regarding gliding arc discharges, Figs. 11 and 12 show small effects

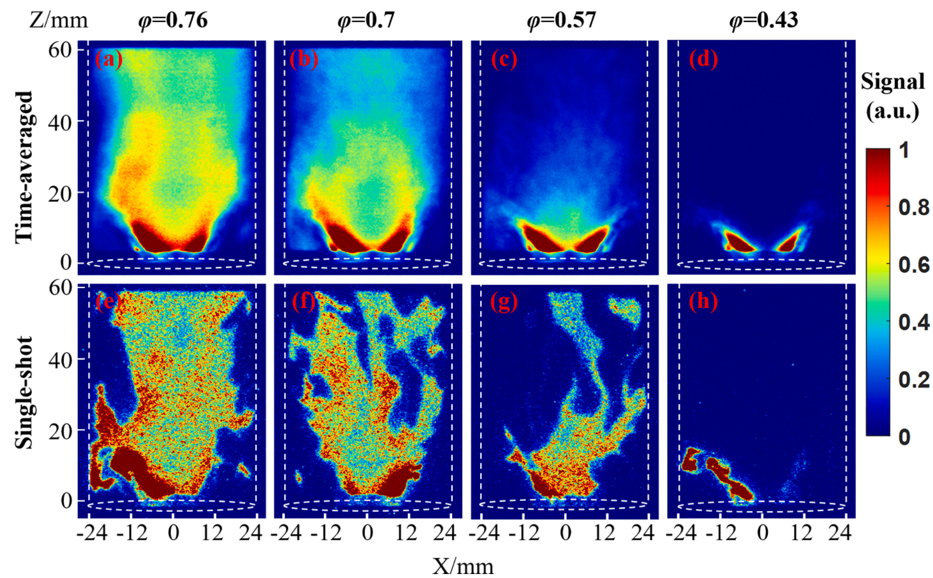

Fig. 10. Time-averaged (a-d) and typical single-shot (e-h) OH PLIF imaging of swirling ammonia/air flames without plasma, at Q_{air} = 50 slm and different equivalence ratios. The outline of the quartz closure is indicated by dashed lines.

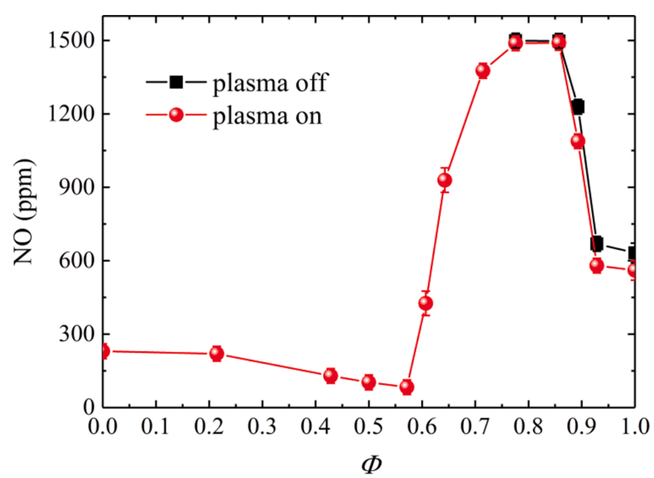

Fig. 11. NO emission of ammonia/air flames with and without plasma (Q_{air} = 50 slm).

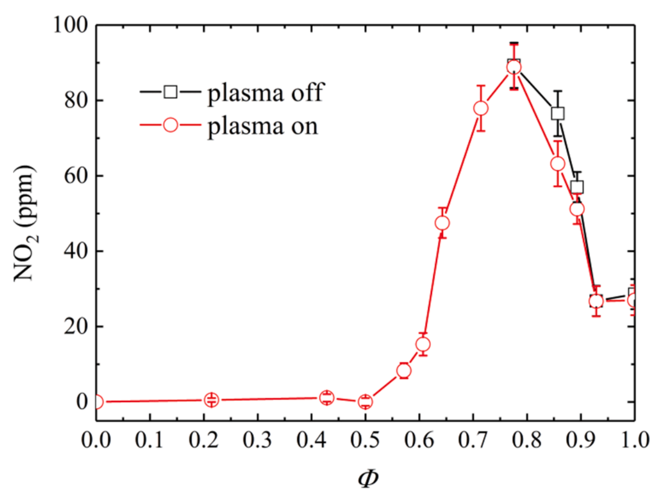

Fig. 12. NO_2 emission of ammonia/air flames with and without plasma (Q_{air} = 50 slm).

of plasma on NO_x emission at equivalence ratios of 0.76–1. Actually, plasma tends to enhance NO_x emission in hydrocarbon combustion [52]. However, NO_x emission in ammonia combustion is more complicated due to the high fuel NO_x. Ref. [42] reported that a larger concentration of NH_2* induced by nanosecond discharges can suppress NO_x emission through the thermal DeNO_x process. The different performance on NO_x reduction is perhaps due to the different properties of nanosecond discharges and AC-powered gliding arc discharges, although both discharges can extend the flammability limit of ammonia swirling combustion to ~ 0.4. In Ref. [42], it was speculated that the reduction of NO results from reactions with HO_2 or NH_2. In this work, NH_2* chemiluminescence and OH PLIF imaging show that gliding arc discharges produce stronger signals of NH_2* and OH. Under the condition approaching flame blow-off (φ = 0.76), the enhancement of NH_2* chemiluminescence is mainly located at the flame root near the plasma column (see Fig. 8e). The enhancement of OH PLIF signals also occurs at the inner recirculation zone and downstream flow (see Fig. 10a). The abundance of NH_2 may trigger NO reduction through the DeNO_x mechanism [6,53–54], and OH can be a direct product of NH_2 + NO reaction.

However, it should be noted that comparing to nanosecond discharges, the gliding arc discharges also have thermal effects [39,55]. Fig. 12 shows a NO_x emission of ~ 230 ppm by discharges in air ($\varphi = 0$). The thermal NO_x emission produced in the high-temperature gas surrounding the plasma column inhibits the NO_x reduction effect. Although the gliding arc discharge can change the flame structure, stability range and flame height through the local ignition effect by the plasma column (*e.g.*, See Figs. 4 and 6), previous studies on methane/air flame showed that the plasma did not change the time-averaged fuel consumption rate and heat release rate [39]. This also suggests a small variation of time-averaged emission from the entire flame in the absence and presence of plasma.

On the other hand, as the gliding arc extends the flammability to very lean conditions, NO_x concentrations decrease rapidly. At $\varphi = 0.57$, NO emission drops to less than 100 ppm, and NO_2 emission drops to nearly zero, which are even smaller than the emission from discharges in the air ($\varphi = 0$). This is mostly due to the NO_x reduction reactions with unburnt NH_3 through the thermal DeNO_x mechanism [53]. Zhang *et al.* [23] verified that the fraction of unburnt ammonia increases quickly as the equivalence ratio drops to 0.7. Here, the high-speed photography (see Fig. 6) shows that at such low equivalence ratios, combustion mainly occurs near the plasma column. Unburnt NH_3 far away from the plasma region can enter into the recirculation zones and reduce NO_x in the downstream hot exhaust. This $DeNO_x$ process is somewhat similar to the reduction by direct ammonia injection into the combustion chamber [56]. Therefore, under the enhancement of plasma, the trade-off relationship between NO and unburnt NH_3 emission indicates that there should be an optimal lean equivalence ratio to achieve the overall minimum emission of ammonia/air combustion. Differing from the rich condition for two-stage ammonia/air combustion [57], plasma-assisted combustion may open a possibility in simultaneous reduction of NO and unburnt NH_3 under fuel-lean conditions.

4. Summary

This work has facilitated AC gliding arc discharges to extend the lean blow-off limits of ammonia/air swirling flames from approximately 0.7–0.8 to 0.3–0.4 in a laboratory-scale burner. Key intermediates such as NH_2* chemiluminescence and O/H/OH were detected by optical inspections, and possible kinetic effects on ammonia combustion have been discussed. The high-frequency repetitive reignition effects of plasma were visualized by high-speed photography, which shows good agreement with our prior work regarding methane/air swirling flames [39].

However, the production of NO_x in ammonia combustion is quite different. Without plasma, NO emissions are positively correlated with the intensity of OH PLIF signals. When the equivalence ratio is 0.8 to 0.85, NO_x emissions reach a peak value of about 1500 ppm. Gliding arc discharges significantly increase NH_2* chemiluminescence that may trigger the thermal $DeNO_x$ process, but show relatively small reduction effects on NO_x in the equivalence range of 0.76–1. This marginal effect is possibly due to the compensation from thermal NO emission induced by gliding arcs. As the equivalence ratio decreases further, NO_x emissions from the plasma-assisted ammonia combustion can drop to less than 100 ppm.

Low NO_x emission under fuel-lean and discharging conditions is expected to result from the reduction effects of unburnt NH_3. Before the implementation of plasma-assisted ammonia combustion in this case, there is a challenge in the simultaneous reduction of NO and unburnt NH_3. Further experimental works including synchronized measurements of NH_3 and NO_x at the hot exhaust should be helpful. It is also noted that, a preliminary test in the current burner indicates that the plasma can also improve the ammonia flammability on the fuel-rich side, which will be carefully studied in future work. Detailed kinetic models will also be attempted to qualify the effects of plasma on ammonia combustion under different conditions.

CRediT authorship contribution statement

Yong Tang: Conceptualization, Methodology, Investigation, Writing – original draft, Funding acquisition. **Dingjiang Xie:** Methodology, Investigation. **Baolu Shi:** Supervision, Writing – review & editing, Funding acquisition. **Ningfei Wang:** Project administration. **Shuiqing Li:** Supervision, Writing – review & editing.

Declaration of Competing Interest

The authors declare that they have no known competing financial interests or personal relationships that could have appeared to influence the work reported in this paper.

Acknowledgments

This work was supported by the National Natural Science Foundation of China (grant numbers 52106129, 91641204) and China Postdoctoral Science Foundation (grant number 2020M680379).

References

[1] Valera-Medina A, Amer-Hatem F, Azad AK, Dedoussi IC, de Joannon M, Fernandes RX, et al. Review on Ammonia as a Potential Fuel: From Synthesis to Economics. Energy Fuel 2021;35(9):6964–7029.
[2] Zamfirescu C, Dincer I. Using ammonia as a sustainable fuel. J Power Sources 2008;185(1):459–65. https://doi.org/10.1016/j.jpowsour.2008.02.097.
[3] Valera-Medina A, Xiao H, Owen-Jones M, David WIF, Bowen PJ. Ammonia for power. Prog Energy Combust Sci 2018;69:63–102. https://doi.org/10.1016/j.pecs.2018.07.001.
[4] E K. Ammonia-a fuel for motor buses. J Inst Pet. 1945; 31: 214-223.
[5] NASA Armstrong Fact Sheet: X-15 Hypersonic Research Program. NASA Armstrong Fact Sheet: X-15 Hypersonic Research Program.
[6] Kobayashi H, Hayakawa A, Somarathne KDKA, Okafor EC. Science and technology of ammonia combustion. Proc Combust Inst 2019;37(1):109–33. https://doi.org/10.1016/j.proci.2018.09.029.
[7] Li J, Lai S, Chen D, Wu R, Kobayashi N, Deng L, et al. A Review on Combustion Characteristics of Ammonia as a Carbon-Free Fuel. Front Energy Res 2021;9:760356. https://doi.org/10.3389/fenrg.2021.760356.
[8] Kurata O, Iki N, Matsunuma T, Inoue T, Tsujimura T, Furutani H, et al. Performances and emission characteristics of NH_3/air and NH_3/CH_4/air combustion gas-turbine power generations. Proc Combust Inst 2017;36(3):3351–9. https://doi.org/10.1016/j.proci.2016.07.088.
[9] Song Y, Hashemi H, Christensen JM, Zou C, Marshall P, Glarborg P. Ammonia oxidation at high pressure and intermediate temperatures. Fuel 2016;181:358–65. https://doi.org/10.1016/j.fuel.2016.04.100.
[10] Pugh D, Runyon J, Bowen P, Giles A, Valera-Medina A, Marsh R, et al. An investigation of ammonia primary flame combustor concepts for emissions reduction with OH*, NH2* and NH* chemiluminescence at elevated conditions. Proc Combust Inst 2021;38(4):6451–9. https://doi.org/10.1016/j.proci.2020.06.310.
[11] Brackmann C, Alekseev VA, Zhou B, Nordström E, Bengtsson P-E, Li Z, et al. Structure of premixed ammonia + air flames at atmospheric pressure: Laser diagnostics and kinetic modeling. Combust Flame 2016;163:370–81. https://doi.org/10.1016/j.combustflame.2015.10.012.
[12] Shu B, Vallabhuni SK, He X, Issayev G, Moshammer K, Farooq A, et al. A shock tube and modeling study on the autoignition properties of ammonia at intermediate temperatures. Proc Combust Inst 2019;37(1):205–11. https://doi.org/10.1016/j.proci.2018.07.074.
[13] Mathieu O, Petersen EL. Experimental and modeling study on the high-temperature oxidation of Ammonia and related NOx chemistry. Combust Flame 2015;162(3):554–70. https://doi.org/10.1016/j.combustflame.2014.08.022.
[14] Wei X, Zhang M, An Z, Wang J, Huang Z, Tan H. Large eddy simulation on flame topologies and the blow-off characteristics of ammonia/air flame in a model gas turbine combustor. Fuel 2021;298:120846. https://doi.org/10.1016/j.fuel.2021.120846.
[15] Somarathne KDKA, Colson S, Hayakawa A, Kobayashi H. Modelling of ammonia/air non-premixed turbulent swirling flames in a gas turbine-like combustor at various pressures. Combust Theor Model 2018;22(5):973–97. https://doi.org/10.1080/13647830.2018.1468035.
[16] Hayakawa A, Arakawa Y, Mimoto R, Somarathne KDKA, Kudo T, Kobayashi H. Experimental investigation of stabilization and emission characteristics of ammonia/air premixed flames in a swirl combustor. Int J Hydrogen Energy 2017;42(19):14010–8. https://doi.org/10.1016/j.ijhydene.2017.01.046.
[17] Chai WS, Bao Y, Jin P, Tang G, Zhou L. A review on ammonia, ammonia-hydrogen and ammonia-methane fuels. Renew Sust Energy Rev. 2021;147:111254. https://doi.org/10.1016/j.rser.2021.111254.
[18] Kumar P, Meyer TR. Experimental and modeling study of chemical-kinetics mechanisms for H_2/NH_3/air mixtures in laminar premixed jet flames. Fuel 2013;108:166–76. https://doi.org/10.1016/j.fuel.2012.06.103.
[19] Okafor EC, Naito Y, Colson S, Ichikawa A, Kudo T, Hayakawa A, et al. Experimental and numerical study of the laminar burning velocity of CH4–NH3–air premixed flames. Combust Flame 2018;187:185–98. https://doi.org/10.1016/j.combustflame.2017.09.002.
[20] Han X, Wang Z, Costa M, Sun Z, He Y, Cen K. Experimental and kinetic modeling study of laminar burning velocities of NH_3/air, NH_3/H_2/air, NH_3/CO/air and NH_3/CH_4/air premixed flames. Combust Flame 2019;206:214–26. https://doi.org/10.1016/j.combustflame.2019.05.003.
[21] Tang G, Jin P, Bao Y, Chai WS, Zhou L. Experimental investigation of premixed combustion limits of hydrogen and methane additives in ammonia. Int J Hydrogen Energy 2021;46(39):20765–76. https://doi.org/10.1016/j.ijhydene.2021.03.154.
[22] Li J, Huang H, Deng L, He Z, Osaka Y, Kobayashi N. Effect of hydrogen addition on combustion and heat release characteristics of ammonia flame. Energy 2019;175:604–17. https://doi.org/10.1016/j.energy.2019.03.075.
[23] Zhang M, An Z, Wang L, Wei X, Jianayihan B, Wang J, et al. The regulation effect of methane and hydrogen on the emission characteristics of ammonia/air combustion in a model combustor. Int J Hydrogen Energy 2021;46(40):21013–25. https://doi.org/10.1016/j.ijhydene.2021.03.210.
[24] An Z, Zhang M, Zhang W, Mao R, Wei X, Wang J, et al. Emission prediction and analysis on CH_4/NH_3/air swirl flames with LES-FGM method. Fuel 2021;304:121370. https://doi.org/10.1016/j.fuel.2021.121370.
[25] Mørch CS, Bjerre A, Gøttrup MP, Sorenson SC, Schramm J. Ammonia/hydrogen mixtures in an SI-engine: Engine performance and analysis of a proposed fuel system. Fuel 2011;90(2):854–64. https://doi.org/10.1016/j.fuel.2010.09.042.
[26] Starikovskiy A, Aleksandrov N. Plasma-assisted ignition and combustion. Prog Energ Combust 2013;39(1):61–110. https://doi.org/10.1016/j.pecs.2012.05.003.

[27] Ju Y, Sun W. Plasma assisted combustion: Dynamics and chemistry. Prog Energ Combust 2015;48:21–83. https://doi.org/10.1016/j.pecs.2014.12.002.

[28] Adamovich IV, Choi I, Jiang N, Kim J-H, Keshav S, Lempert WR, et al. Plasma assisted ignition and high-speed flow control: non-thermal and thermal effects. Plasma Sources Sci Technol 2009;18(3):034018. https://doi.org/10.1088/0963-0252/18/3/034018.

[29] Tang Y, Yao Q, Zhuo J, Li S. Plasma-assisted pyrolysis and ignition of pre-vaporized n-heptane, iso-octane and n-decane. Fuel 2021;289:119899. https://doi.org/10.1016/j.fuel.2020.119899.

[30] Mao X, Rousso A, Chen Q, Ju Y. Numerical modeling of ignition enhancement of CH4/O2/He mixtures using a hybrid repetitive nanosecond and DC discharge. Proc Combust Inst 2019;37(4):5545–52. https://doi.org/10.1016/j.proci.2018.05.106.

[31] Tang Y, Zhuo J, Cui W, Li S, Yao Q. Enhancing ignition and inhibiting extinction of methane diffusion flame by in situ fuel processing using dielectric-barrier-discharge plasma. Fuel Process Technol 2019;194:106128. https://doi.org/10.1016/j.fuproc.2019.106128.

[32] Sun W, Uddi M, Won SH, Ombrello T, Carter C, Ju Y. Kinetic effects of non-equilibrium plasma-assisted methane oxidation on diffusion flame extinction limits. Combust Flame 2012;159(1):221–9. https://doi.org/10.1016/j.combustflame.2011.07.008.

[33] Kim W, Snyder J, Cohen J. Plasma assisted combustor dynamics control. Proc Combust Inst 2015;35(3):3479–86. https://doi.org/10.1016/j.proci.2014.08.025.

[34] Varella RA, Sagás JC, Martins CA. Effects of plasma assisted combustion on pollutant emissions of a premixed flame of natural gas and air. Fuel 2016;184:269–76. https://doi.org/10.1016/j.fuel.2016.07.031.

[35] Lin B, Wu Y, Zhu Y, Song F, Bian D. Experimental investigation of gliding arc plasma fuel injector for ignition and extinction performance improvement. Appl Energy 2019;235:1017–26. https://doi.org/10.1016/j.apenergy.2018.11.026.

[36] An B, Yang L, Wang Z, Li X, Sun M, Zhu J, et al. Characteristics of laser ignition and spark discharge ignition in a cavity-based supersonic combustor. Combust Flame 2020;212:177–88. https://doi.org/10.1016/j.combustflame.2019.10.030.

[37] Cui W, Ren Y, Li S. Stabilization of Premixed Swirl Flames Under Flow Pulsations Using Microsecond Pulsed Plasmas. J Propul Power 2019;35(1):190–200. https://doi.org/10.2514/1.B37219.

[38] Sun J, Tang Y, Li S. Plasma-assisted Stabilization of Premixed Swirl Flames by Gliding Arc Discharges. Proc Combust Inst 2020;38(4):6733–41. https://doi.org/10.1016/j.proci.2020.06.223.

[39] Tang Y, Sun J, Shi B, Li S, Yao Q. Extension of flammability and stability limits of swirling premixed flames by AC powered gliding arc discharges. Combust Flame 2021;231:111483. https://doi.org/10.1016/j.combustflame.2021.111483.

[40] Shioyoke A, Hayashi J, Murai R, Nakatsuka N, Akamatsu F. Numerical Investigation on Effects of Nonequilibrium Plasma on Laminar Burning Velocity of Ammonia Flame. Energy Fuel 2018;32(3):3824–32. https://doi.org/10.1021/acs.energyfuels.7b02733.

[41] Faingold G, Lefkowitz JK. A numerical investigation of NH_3/O_2/He ignition limits in a non-thermal plasma. Proc Combust Inst 2021;38(4):6661–9. https://doi.org/10.1016/j.proci.2020.08.033.

[42] Choe J, Sun W, Ombrello T, Carter C. Plasma assisted ammonia combustion: Simultaneous NOx reduction and flame enhancement. Combust Flame 2021;228:430–2. https://doi.org/10.1016/j.combustflame.2021.02.016.

[43] Shi B, Shimokuri D, Ishizuka S. Methane/oxygen combustion in a rapidly mixed type tubular flame burner. Proc Combust Inst 2013;34(2):3369–77. https://doi.org/10.1016/j.proci.2012.06.133.

[44] Tang Y, Yao Q, Cui W, Pu Y, Li S. Flow fluctuation induced by coaxial plasma device at atmospheric pressure. Appl Phys Lett 2018;113(22):224101. https://doi.org/10.1063/1.5063486.

[45] Gao J, Kong C, Zhu J, Ehn A, Hurtig T, Tang Y, et al. Visualization of instantaneous structure and dynamics of large-scale turbulent flames stabilized by a gliding arc discharge. Proc Combust Inst 2019;37(4):5629–36. https://doi.org/10.1016/j.proci.2018.06.030.

[46] Massa L, Freund JB. Plasma-combustion coupling in a dielectric-barrier discharge actuated fuel jet. Combust Flame 2017;184:208–32. https://doi.org/10.1016/j.combustflame.2017.06.008.

[47] Zhu X, Khateeb AA, Roberts WL, Guiberti TF. Chemiluminescence signature of premixed ammonia-methane-air flames. Combust Flame 2021;231:111508. https://doi.org/10.1016/j.combustflame.2021.111508.

[48] Zhu J, Ehn A, Gao J, Kong C, Aldén M, Salewski M, et al. Translational, rotational, vibrational and electron temperatures of a gliding arc discharge. Opt Express 2017;25(17):20243. https://doi.org/10.1364/OE.25.020243.

[49] Miller JA, Smooke MD, Green RM, Kee RJ. Kinetic Modeling of the Oxidation of Ammonia in Flames. Combust Sci Technol 1983;34(1–6):149–76. https://doi.org/10.1080/00102208308923691.

[50] Gaydon AG. The spectroscopy of flames. second ed. London Chapman and Hall; 1974.

[51] Somarathne KDKA, C. Okafor E, Hayakawa A, Kudo T, Kurata O, Iki N, et al. Emission characteristics of turbulent non-premixed ammonia/air and methane/air swirl flames through a rich-lean combustor under various wall thermal boundary conditions at high pressure. Combust Flame 2019;210:247–61. https://doi.org/10.1016/j.combustflame.2019.08.037.

[52] Xiong Y, Schulz O, Bourquard C, Weilenmann M, Noiray N. Plasma enhanced auto-ignition in a sequential combustor. Proc Combust Inst 2019;37(4):5587–94. https://doi.org/10.1016/j.proci.2018.08.031.

[53] Lyon RK. The NH_3-NO-O_2 reactions. Int J Chem Kinet 1976;8(2):315–8.

[54] Miller JA, Pilling MJ, Troe J. Unravelling combustion mechanisms through a quantitative understanding of elementary reactions. Proc Combust Inst 2005;30(1):43–88. https://doi.org/10.1016/j.proci.2004.08.281.

[55] Kong C, Li Z, Aldén M, Ehn A. Thermal analysis of a high-power glow discharge in flowing atmospheric air by combining Rayleigh scattering thermometry and numerical simulation. J Phys D Appl Phys 2020;53(8):85502. https://doi.org/10.1088/1361-6463/ab586f.

[56] Nam CM, Gibbs BM. Application of the thermal DeNOx process to diesel engine DeNOx:an experimental and kinetic modelling studyq. Fuel 2002;81:1359–67.

[57] Somarathne KDKA, Hatakeyama S, Hayakawa A, Kobayashi H. Numerical study of a low emission gas turbine like combustor for turbulent ammonia/air premixed swirl flames with a secondary air injection at high pressure. Int J Hydrogen Energy 2017;42(44):27388–99. https://doi.org/10.1016/j.ijhydene.2017.09.089.